Thermodynamics and Kinetics of Hydroxide Ion Formation in $12CaO \cdot 7Al_2O_3$

Katsuro Hayashi,* Masahiro Hirano, and Hideo Hosono†

Frontier Collaborative Research Center, Tokyo Institute of Technology, S2−13, 4259 Nagatsuta, Yokohama 226-8503, Japan

Received: February 16, 2005; In Final Form: April 23, 2005

We have examined the thermodynamics and kinetics of hydroxide (OH^-) ions that formed in cages of $12CaO \cdot 7Al_2O_3$ (C12A7) with nanoporous structures. It is confirmed using thermogravimetric-evolved gas analyses (TG-EGA) that hydration in C12A7 is mediated by a reaction between an oxide (O^{2-}) ion in the cage and an H_2O molecule in the atmosphere to form two OH^- ions in the cages. To simply and exactly quantify the OH^- content from infrared absorption measurements of OH-stretching band, we propose a method combined with a thermodynamic analysis, allowing the simultaneous determination of the molar extinction coefficient of the OH-band, enthalpy, and entropy for the hydration. Hydration enthalpy in C12A7 is extremely high compared with other oxides and was enhanced by the marked instability of O^{2-} ion in the cage. Consequently, high solubility of OH^- ion is retained up to unusually high temperatures. Furthermore, we determined diffusion coefficients of species relevant to the hydration process and demonstrated that inward diffusion of OH^- ions is the rate-determining process.

1. Introduction

Incorporation of "zeolitic water" into $12CaO \cdot 7Al_2O_3$ (C12A7) has been accepted for a long time as observed by a simultaneous weight loss and water desorption without any crystal structure changes when C12A7 was heated at temperatures higher than ∼1000 °C in ambient atmosphere.[1] On the contrary, water uptake occurs when C12A7 is heated to temperatures of ∼ 400−900 °C. These behaviors have been ascribed to the combination of the nanoporous lattice framework inherent to C12A7 (Figure 1) with the presence of extra-framework O^{2-} ions that are encapsulated in the cages.[2] Under these conditions, water reacts with O^{2-} ions to form OH^- ions in the cages. That is, hydration and dehydration occur reversibly following the reaction:

$$(Ca_{12}Al_{14}O_{32})^{2+} \cdot O^{2-} + H_2O \leftrightarrow (Ca_{12}Al_{14}O_{32})^{2+} \cdot 2(OH)^- \quad (1)$$

where $(Ca_{12}Al_{14}O_{32})^{2+}$ indicates the lattice framework, and O^{2-} and OH^- are the extra-framework anions. Other than OH^- ions, several kinds of extrinsic anions including F^-, Cl^-,[3] O_2^-,[4] O^-,[5] H^-,[6] S^{2-},[7] and C_2^{2-} [8] were proved or suggested to selectively substitute for the extra−framework O^{2-} ions. Moreover, the electron can even act as the substitutional anion.[9] Subsequently, these extrinsic anions could act as potential origins of novel functionalities for C12A7.[10−13]

The OH^- ion is the most common extrinsic anion in C12A7 since ambient water works as a precursor, frequently leading to unintentional formation of OH^- ions. In addition, OH^- ions markedly influence the apparent properties of C12A7: (1) OH^- ions are retained up to unusually high-temperatures, markedly affecting its sintering behavior;[14] (2) although intrinsic C12A7 has an excellent infrared (IR) transmission up to a wavelength of 6−10 μm, an absorption band due to the OH-stretching mode deteriorates the IR transparency of C12A7; (3) the presence of OH^- ions masks the intrinsic properties of C12A7 such as fast oxide ionic conduction[10] and hinders the incorporation of extrinsic anions, for instance the formation of oxygen radicals or electrons in cages is remarkably reduced by the presence of OH^- ions.[5,15] Thus, elimination of OH^- ions is crucial for the realization of new functionalities by the incorporation of extrinsic anions. However, neither quantification methods nor the thermodynamic nature of OH^- ions have been established yet.

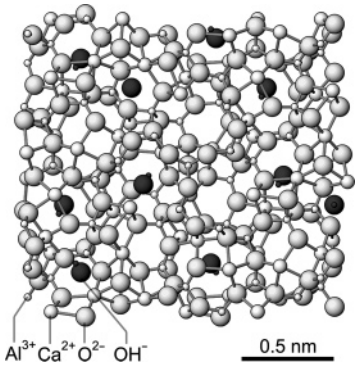

Figure 1. Crystal structure of $12CaO \cdot 7Al_2O_3$ showing the nanoporous lattice framework and the OH^- ion encapsulated inside the cage structure.

Generally, measurement of the IR OH-stretching band allows a more accurate quantification of OH^- concentration than other methods such as weight change or mass spectroscopy. However, the molar integral extinction coefficient *A* of the OH-band has not yet been determined in C12A7. In this study, we first confirm the hydration-dehydration reaction described by eq 1 using thermogravimetric-evolved gas analyses. Next, infrared (IR) OH-band is precisely measured to obtain relative concentrations of OH^- ions in samples as a function of temperature and water vapor pressure $p(H_2O)$. The obtained data are

* To whom correspondence should be addressed. E-mail: k-hayashi@lucid.msl.titech.ac.jp

† Also at Materials and Structures Laboratory, Tokyo Institute of Technology.

10.1021/jp050807j CCC: $30.25
Published on Web 05/26/2005

analyzed thermodynamically on the basis of eq 1, making it possible to determine the *A* value together with the thermodynamic parameters for the OH^- formation. Furthermore, the kinetics of the OH^- formation is examined by analyzing time-evolution characteristics of the OH-band during isothermal annealing.

2. Experimental Section

2.1. Thermogravimetric-Evolved Gas (TG-EG) Analyses. C12A7 powder was prepared by a solid-state reaction of reagent-grade $CaCO_3$ and γ-Al_2O_3 powders at 1350 °C for 6 h in air. Then, the C12A7 powder was crushed by planetary ball milling with alumina balls as a crushing media and ethanol as a solvent. Relative surface area of the crushed powder was 2.7 $m^2{\cdot}g^{-1}$ as measured by the BET analysis. The powder was subsequently annealed at 1000 °C for 2 h in an alumina-tube furnace in a "wet" atmosphere, where $p(H_2O)$ was maintained at 0.02 atm by He gas flow after passing through a humidifier. The value of $p(H_2O)$ was measured using a dew-point meter. About 30 mg of the wet-treated powder was used for the thermogravimetric-evolved gas (TG-EG) analyses using a Rigaku Thermoplus system. The carrier gas in an alumina-tube furnace of the TG-EG system was supplied through the same humidification system. Weight changes in dry He with $p(H_2O) < 5 \times 10^{-4}$ atm were recorded with an increase in temperature from room temperature to 1350 °C with a heating rate of 600 $K{\cdot}h^{-1}$. Simultaneously, water desorption was measured with a quadrupole mass spectrometer by monitoring a mass peak at $m/e = 18$. In addition, weight changes in humidified He with $p(H_2O) = 1 \times 10^{-3}$ atm were recorded during heating to 1350 °C with +600 $K{\cdot}h^{-1}$, holding at 1350 °C for 2 h, and cooling from 1350 °C with −100 $K{\cdot}h^{-1}$.

2.2. IR Absorption of OH-Stretching Band. Transparent C12A7 polycrystalline ingots refined by the floating zone method were used for IR absorption measurements. They were sliced into ~3 × 3 mm pieces. The slices were ground and polished to ~200 μm thick plates with mirror surfaces using oleaginous diamond paste. Each sample was composed of several grains with different crystal orientations, and hence the crystal axis with respect to light polarization was not accounted for in the present study. The initial OH^- concentration was ~2.0×10^{19} cm^{-3}, which was evaluated after the determination of the *A* value as described in the following sections. An alumina tube furnace equipped with the same humidification system as that of the TG-EG analyses was used for annealing the samples under $p(H_2O)$ ranging from 0.02 to 1×10^{-3} atm. For isothermal annealing, samples were quickly transferred to a hot zone heated at 1000, 1200, or 1350 °C, held from 10 min to 80 h, followed by quenching to room temperature by immediately transferring the samples to a water-cooled zone of the tube furnace. Optical spectra were measured using a Hitachi U4000 spectrophotometer and a Perkin-Elmer Spectrum One FT-IR spectrometer at room temperature.

2.3. Electron Paramagnetic resonance. Electron paramagnetic resonance (EPR) measurements were performed at ~9.7 GHz (X-band) using a Bruker E580 spectrometer. The spin concentrations in the samples were determined from the second integral of the spectra using $CuSO_4{\cdot}5H_2O$ as a standard.

3. Results

3.1. TG-EG Analyses. Figure 2 shows TG-EG analyses of the wet-treated C12A7 powder. Weight loss more than 1% was observed during heating from ~ 500 °C to 1350 °C, and nearly equal amounts of the weight were recovered by cooling from

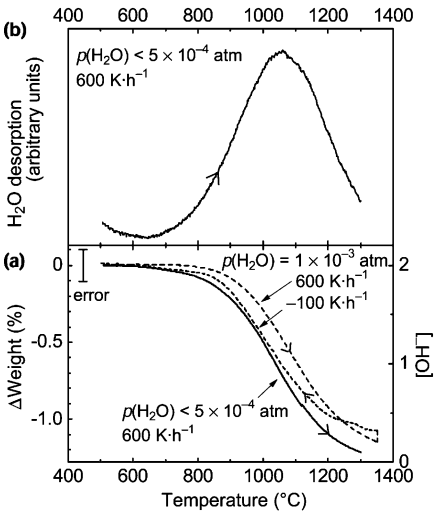

Figure 2. Thermogravimetric-evolved gas (TG-EG) analyses of C12A7 powder preheated at 1000 °C in wet He with $p(H_2O) = 0.02$ atm. (a) Weight loss as a function of temperature. Solid line was recorded during heating with +600 $K{\cdot}h^{-1}$ in dry He with $p(H_2O) < 5 \times 10^{-4}$ atm. Dashed line was recorded during heating with +600 $K{\cdot}h^{-1}$, holding at 1350 °C for 2h, and cooling with −100 $K{\cdot}h^{-1}$ in humidified He with $p(H_2O) = 1 \times 10^{-3}$ atm. (b) Intensity of $m/e = 18(H_2O)$ measured by quadrapole mass spectroscopy during heating with +600 $K{\cdot}h^{-1}$ in dry He as a function of temperature.

1350 °C to ~ 500 °C in humidified He with $p(H_2O) = 1 \times 10^{-3}$ atm (Figure 2a). Water desorption (Figure 2b) well correlated with weight loss during the heating process, clearly indicating that the weight changes were due to the release and uptake of water.

As indicated in eq 1, since the maximum water uptake corresponds to the formation of two extra-framework OH^- ions per one molecule of C12A7, the complete dehydration should result in a weight loss of 1.28%, which is close to the observed weight loss of ~1.2%. This agreement supports the formation of the extra-framework OH^- ions in the cages and further suggests that the hydration or dehydration occurs almost completely during the heating or cooling process between ~500 °C and 1350 °C.

TG-EG analyses qualitatively validated that uptake of water is due to the formation of OH^- ions in the cages. However, these analyses were not accurate enough to quantitatively determine the OH^- content. Alternatively, we employ a combined procedure of IR measurements with thermodynamic analyses for quantifying OH^- content in C12A7 in the next section.

3.2. Thermodynamics of OH^- Ion Formation and Determination of Molar Integral Extinction Coefficient of OH Stretching Vibration Mode. Figure 3 shows IR absorption spectra of samples equilibrated by isothermal annealing. The time required to reach the equilibrated concentration was judged from the saturation behavior in the growth of the absorption band intensity due to the OH-stretching mode. Details will be discussed in a later section. The fundamental OH-stretching band was observed at ~3200−4000 cm^{-1} with a peak at ~3540 cm^{-1}. The inset of Figure 3 shows the absorption spectrum in the lower energy range. The main peak that appears at ~830 cm^{-1}, which is assigned to the asymmetrical stretching of AlO_4 tetrahedrons with the nonbridging oxygen,[16] is to be combined with the fundamental band to generate a combination band at 4370 cm^{-1}. We observed neither the OH-deformation band, which is possibly located at ~1700 cm^{-1}, nor its combination band with the fundamental band. These facts confirmed the absence of

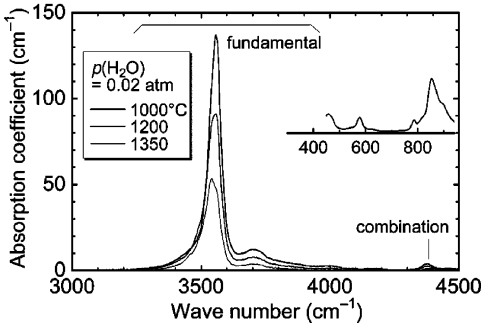

Figure 3. Absorption spectra of OH-stretching band for various samples equilibrated in wet He with $p(H_2O) = 0.02$ atm. The peak of the fundamental band is located at ~3540 cm^{-1}. The inset shows absorption spectrum at the lower energy range obtained by the Kramers−Kronig transformation of the reflection spectrum. A band peaking at ~830 cm^{-1} is coupled to the fundamental band to generate a combination band at 4370 cm^{-1}.

molecular water in the samples. Thus, the integral extinction coefficient, $\int \epsilon \, d\nu$, for the OH-stretching band was evaluated from signals at ~3200−4000 cm^{-1}, where ϵ (cm^{-1}) is the extinction coefficient and ν (cm^{-1}) is the wave number.

Molar fraction of OH^- ion, [OH^-], is described by

$$[OH^-] = \frac{N_A}{1000 c_a A} \int \epsilon \, d\nu \tag{2}$$

where, N_A is the Avogadro number (6.02×10^{23}), c_a is the molar concentration of extra-framework anions (1.16×10^{21} cm^{-3}). This relationship directly gives the absolute value of [OH^-] from the IR spectra, if the A value is determined.

On the other hand, [OH^-] is described thermodynamically as follows. The formation of OH^- ions as a result of the reaction of the extra-framework O^{2-} ion with water is

$$O^{2-}(\text{cage}) + \text{null}(\text{cage}) + H_2O(g) \leftrightarrow 2OH^-(\text{cage}) \tag{3}$$

where (cage) denotes chemical species in cages and null the empty cages. The equilibrium constant for eq 3 is written as

$$K = \frac{[OH^-]^2}{[O^{2-}][\text{null}]p(H_2O)} \tag{4}$$

where the brackets denote the molar fraction of corresponding species. All chemical species in the cages are assumed to be ideal solutions, and water vapor an ideal gas. The charge neutrality condition restricts the cage constituents as

$$2[O^{2-}] + [OH^-] = 2 \tag{5}$$

That is, to compensate the positive charge of the lattice, one molecule of C12A7 should incorporate extra-framework anion(s) whose total charge is equal to two elemental charges. Oxygen radicals such as O_2^- and O^- are ignored, because EPR measurement revealed that their total concentration is less than 10^{17} cm^{-3}, which corresponds to a molar fraction less than 10^{-4}. Since the number of cages per one molecule of C12A7 is 6, the site restriction of the cage gives

$$[O^{2-}] + [OH^-] + [\text{null}] = 6 \tag{6}$$

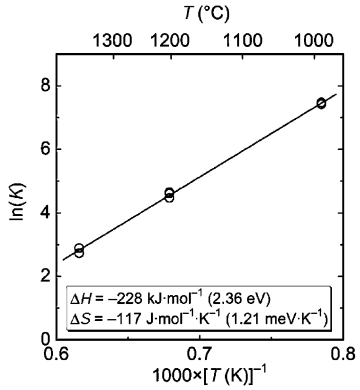

Figure 4. Result of least-squares fit of eq 8 (Van't Hoff plot) for experimentally evaluated K value which is a function of A as in eqs 2 and 7.

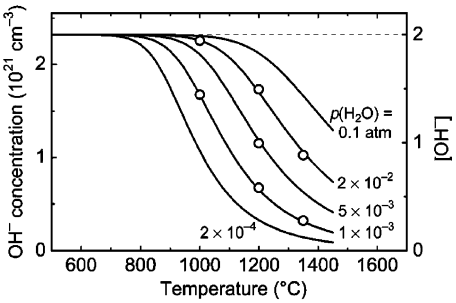

Figure 5. Temperature and $p(H_2O)$ dependence of equilibrium [OH^-]. Open circles and solid lines denote experimental and theoretical values, respectively.

From eqs 4, 5 and 6, K is rewritten as

$$K = \frac{4[OH^-]^2}{(2 - [OH^-])(10 - [OH^-])p} \tag{7}$$

The K value is expressed as a function of A by substituting eq 2 for [OH^-] in eq 7. On the other hand, temperature dependence of K is described as

$$\ln K = \Delta H/RT - \Delta S/R \tag{8}$$

where R is the gas constant, T is the absolute temperature, and ΔH and ΔS are the enthalpy and the entropy for the hydration, respectively. Temperature dependences of ΔH and ΔS are, in general, so small in a restricted temperature range that they are treated as constants.

Now, there are three unknown parameters: A, ΔH, and ΔS. To determine these values, we measured the integral extinction coefficient of the OH-band in seven samples equilibrated under different temperature and $p(H_2O)$ conditions. Then, the values of the three unknown parameters can be determined by the least-squares method. As shown in Figure 4, eq 8 was applied to the K value using the least-squares method to calculate the three unknown values. A good linear relationship was obtained between ln K and $1/T$. From this result, we obtained −228 kJ·mol^{-1} (2.36 eV) for ΔH, −117 J·mol^{-1}·K^{-1} (1.21 meV·K^{-1}) for ΔS, and 1.31×10^3 M^{-1}·cm^{-2} for A.

Solid lines in Figure 5 show the calculated [OH^-] for various $p(H_2O)$ as a function of temperature using the optimized A, ΔH, and ΔS, and the following equation, which is converted from eq 7:

$$[OH^-] = \frac{4\sqrt{K^2p^2 + 5Kp} - 6Kp}{4 - Kp} \tag{9}$$

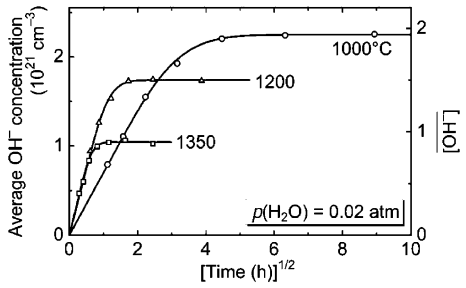

Figure 6. Time evolution of the changes in the average OH^- ion content, $[\overline{OH^-}]$, for samples annealed under $p(H_2O) = 0.02$ atm at 1000, 1200, and 1350 °C. Solid lines are theoretical curves given by eq 9 with best fitted results.

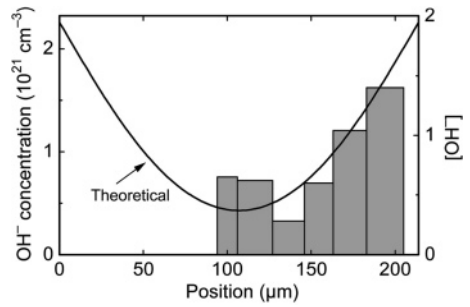

Figure 7. Depth profile of OH^- content in a sample annealed at 1000 °C for 3 h under $p(H_2O) = 0.02$. The OH^- content at a given depth was estimated by the repeat of sample grinding and measurments of OH-stretching band intensity. Initial thickness was 214 μm. Solid line corresponds to the theoretical distribution curve given by eq 10.

In Figure 5, experimental values converted using the optimized A are shown by open circles, which agree very well with theoretical curves. Furthermore, it is found that temperature dependence of $[OH^-]$ under $p(H_2O) = 1 \times 10^{-3}$ atm reasonably agrees with the TG analysis shown in Figure 2, further validating that the hydration reaction proceeds via eq 3.

3.3. Kinetics of H_2O Uptake. In the previous sections, the hydration reaction was identified as eq 3 and the absence of molecular water in the lattice framework was demonstrated. Therefore, the water uptake process most likely occurs with following three steps: (1) outward diffusion of an extra-framework O^{2-} ion to the surface, (2) reaction of an O^{2-} ion with an H_2O molecule in the atmosphere at the surface to form a pair of OH^- ions, and (3) inward diffusion of OH^- ions. Thus, the total process is regarded as a chemical inward diffusion of H_2O. We determined the chemical diffusion coefficient for H_2O from the time-evolution of the OH-stretching band during isothermal annealing.

Before equilibration is established by isothermal annealing, OH^- distribution in the sample is nonuniform. Thus, $[OH^-]$ value measured by the IR absorption corresponds to that of the averaged value in the sample, $[\overline{OH^-}]$. Then, $[\overline{OH^-}]/2$ gives the average molar fraction of H_2O incorporated into the sample. Open circles in Figure 6 show experimental data. Saturation of the $[\overline{OH^-}]$ value with prolonged annealing time indicates that the formation of OH^- ions has reached an equilibrium.

Provided that the bulk diffusion process rather than the surface reaction is the rate-determining step for the total water uptake process, and the OH^- content at the surface is always in equilibrium with atmosphere, the total uptake of water in a planner sample is given by[17]

$$\frac{\overline{[OH^-]}}{[OH^-]_{eq}} = 1 - \sum_{n=0}^{\infty} \frac{8}{(2n+1)^2\pi^2} \exp\left\{-\frac{\tilde{D}_{H_2O}(2n+1)^2\pi^2 t}{(2l)^2}\right\} \quad (10)$$

where $[OH^-]_{eq}$ is the equilibrium value of $[OH^-]$, $\tilde{D}_{H_2O}$ is the chemical diffusion coefficient of H_2O, $2l$ is the thickness of sample, and t is the time. Solid lines in Figure 6 are for theoretical curves calculated using eq 10. The excellent fit between the theoretical curves and the experimental points confirms that the bulk diffusion is the rate-determining process for the water uptake. This conclusion is further supported by

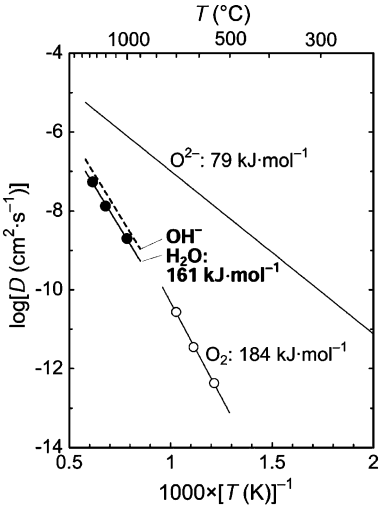

Figure 8. Arrhenius plot of the chemical diffusion coefficient of H_2O and the diffusion coefficient of OH^- together with the diffusion coefficient of O^{2-} ion and the chemical diffusion coefficient of O_2.[18]

Figure 7, where the depth profile of $[OH^-]$ is plotted together with the theoretical curve calculated by

$$\frac{[OH^-]}{[OH^-]_{eq}} = 1 - \frac{4}{\pi}\sum_{n=0}^{\infty} \frac{(-1)^n}{2n+1} \exp\left\{-\frac{\tilde{D}_{H_2O}(2n+1)^2\pi^2 t}{(2l)^2}\right\} \cos\frac{(2n+1)\pi x}{2l} \quad (11)$$

which is obtained under the conditions that the bulk diffusion is the rate-determining process,[17] and x ($-l \le x \le l$) indicates the depth in the sample. Experimental data show reasonable agreement with the theoretical curve.

Figure 8 represents the Arrhenius plot of the diffusion coefficient, $\tilde{D}_{H_2O}$, of H_2O obtained by the theoretical fit in Figure 6. Temperature dependence of $\tilde{D}_{H_2O}$ is described by the following equation:

$$\tilde{D}_{H_2O} = 7.6 \times 10^{-3\pm0.1} \exp\left(-\frac{161 \pm 5 \text{kJ·mol}^{-1}}{RT}\right) \quad (12)$$

In Figure 8, the diffusion coefficient for O^{2-} ions and chemical diffusion coefficient for O_2[18] are plotted for comparison. The chemical diffusion coefficient of water is smaller by 2−3 orders of magnitude than the diffusion coefficient of the O^{2-} ions and it is also smaller within 1 order of magnitude than that of O_2 at

TABLE 1: Molar Integral Extinction Coefficient *A*, and Molar Extinction Coefficient ϵ_p, at Peak of of the OH-stretching band

substance		A ($M \cdot cm^{-2}$)	ϵ_p($M \cdot cm^{-1}$)	Reference
Alkali halides	NaCl	2.71×10^2	−	20
	NaBr	2.08×10^2	−	20
	KCl	1.50×10^3	−	20
	KCl	2.15×10^3	−	26
	RbCl	2.37×10^3	−	20
	KBr	1.43×10^3	−	20
	KI	9.53×10^2	−	20
α-Al_2O_3		3.10×10^3	−	27
TiO_2 (rutile)		3.58×10^4	−	21
SiO_2 glass		2.11×10^4	38.7	28
		2.15×10^4 [a]	71[a]	29
		−	90.5	22
Hydroxyl group in H_2O		1.95×10^4	46[a]	30
C12A7		$1.31(\pm 0.04) \times 10^3$	14.8($\pm$0.1)	Present work

[a] Evaluated by the present authors from published data.

the equivalent measured temperature range. This result indicates that the inward diffusion of OH^- ions rather than the outward diffusion of O^{2-} ion is the rate determining process for the formation of OH^-.

4. Discussion

4.1. Molar Extinction Coefficient of OH-Stretching Band. So far, the molar extinction coefficient of OH^- ions, *A*, in solids has been determined by the measurement of IR OH-stretching band combined with the measurement of desorbed gases,[19] by pH titration,[20] by weight change by hydrogen−deuterium exchange,[21] or by weight change by H_2O uptake,[22] etc. The method used in the present study shows advantages over previous methods: (1) both molar extinction coefficient and thermodynamic parameters can be simultaneously obtained and (2) only the measurement of the OH-stretching band is a requisite. However, the accuracy of the *A* value estimated by the current method depends on the validity of the assumptions made in the thermodynamic evaluation process, especially on whether chemical species in cages behave as ideal solutions or not. In the case of C12A7, extra-framework species are isolated from each other by the lattice framework, therefore their interactions are weak enough to be treated as the ideal solution.

Although the evaluation of *A* has been validated by a reasonable agreement between the TG-EG results and the IR spectroscopic-thermodynamic analysis, we have made an additional check of its accuracy. That is, $[O^{2-}]$ in several samples was determined from ultraviolet (UV) absorption at 4−6 eV. It was found that the relationship between $[O^{2-}]$ and $[OH^-]$ was in accordance with the charge neutrality condition of the extra-framework species given by eq 5. From this result, the error in the *A* value was estimated to be within a few percent ($A = 1.31 \pm 0.04 \times 10^3$ $M^{-1} \cdot cm^{-2}$). Details of the UV-absorption will be reported elsewhere.[23] By accounting for the error in the *A* value, errors in the ΔH and ΔS values were estimated to be -228 ± 20 $kJ \cdot mol^{-1}$ and -117 ± 10 $J \cdot mol^{-1} \cdot K^{-1}$, respectively.

The molar extinction coefficient ϵ_p, at the peak of the IR OH-stretching band has been commonly used for estimating OH^- concentration in various materials.[19,22,28] The value of ϵ_p for C12A7 was calculated as 14.8 ± 1.0 $M^{-1} \cdot cm^{-1}$ from a linear relationship between the integral extinction coefficient and the extinction coefficient at the peak. This value is about six times smaller than that for SiO_2 ($\epsilon_p = 90.5$ $M^{-1} \cdot cm^{-1}$)[22] and has been applied to C12A7 in previous reports.[6,14] Thus the previous estimation of OH^- concentrations were possibly underestimated.

Table 1 summarizes *A* and ϵ_p values at the peak height of the OH-stretching band for various materials. The *A* value for C12A7 is comparable to those for alkali halides and significantly smaller than those for other oxides.

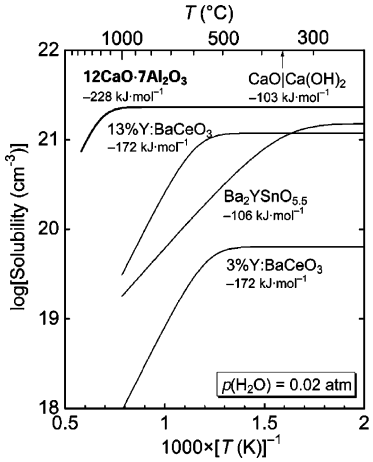

Figure 9. Solubility of OH^- ions calculated using thermodynamic parameters for C12A7 and for protonic conductors[24] under $p(H_2O) = 0.02$ atm. Arrow indicates dehydration temperature of $Ca(OH)_2$ obtained from thermodynamic data.[25] Values in the figure show hydration enthalpy.

4.2. Solubility of OH^- Ion. Figure 9 compares the solubility of OH^- ions in C12A7 with typical high-performance protonic conductors, which retain high concentration of OH^- ions at elevated temperatures, thereby providing considerable high-temperature protonic conductivity. It is noted that the solubility of OH^- ions in C12A7 exceeds those in the protonic conductors.[24] The dehydration temperature for C12A7 (~1200 °C) is also much higher than those for protonic conductors or $Ca(OH)_2$ (~350−700 °C),[25] which resulted from the extremely high hydration enthalpy in C12A7.

The origin of the high hydration enthalpy in C12A7 is likely explained in terms of the instability of the extra-framework O^{2-} ions as it has been discussed for the formation of oxygen radicals in C12A7.[18] The O^{2-} ions in the gas phase are unstable due to the very large positive second electron affinity of the oxygen, while O^{2-} ions in ionic crystals are stabilized due to the Madelung potential. In the case of C12A7, only 1/3 of elemental charge is allocated to each cage, and the free space inside the cage (~0.4 nm in diameter) is larger by ~40% as compared with an ordinary O^{2-} site in ionic crystals. Thus, O^{2-} inside the cage has an intermediate stability between that in the gas phase and that in the ionic crystal, leading to a higher hydration enthalpy than those in other oxide systems.

The unusual high solubility, especially at higher temperatures, may provide practical applications such as a desiccating agent or a moisture restorer that can operate at high temperatures. In addition, the temperature range for the dehydration (~1200−1400 °C) agrees with the sintering temperature of C12A7, implying that sintering may be markedly affected by the presence of the extra-framework OH^- ions or $p(H_2O)$ in atmosphere. In fact, the importance of water for the fabrication of the translucent ceramics has been observed in our previous study.[14]

4.3. Diffusivity of OH^- Ions. Chemical inward diffusion of an H_2O molecule is well described as an ambipolar diffusion consisting of the outward diffusion of an O^{2-} ion and the inward diffusion of two OH^- ions. The chemical diffusion coefficient of water is much smaller than the diffusion coefficient of an O^{2-} ion. Thus, as derived from the Appendix, the diffusion coefficient D_{OH^-} of an OH^- ion is approximated to be $2\tilde{D}_{H_2O}$, which is plotted as a dashed line in Figure 8.

During intercage migration of the OH^- ion, the OH^- ion may further dissociate into O^{2-} ion and proton. Then, the O^{2-} ion migrates as fast as the other extra-framework O^{2-} ions, while the proton may bond to a framework O^{2-} ion and migrates by the switching of the O−H bond to another framework O^{2-} ion. Debonding of OH^- ion and proton hopping processes probably dominate the diffusion of the OH^- ions. Hence, the observed activation energy of $\tilde{D}_{H_2O}$ may correspond either to the energy barriers for the debonding and the proton migration processes. If this is the case, the proton conductivity in the fully hydrated C12A7 will be about 2 orders of magnitude less than the O^{2-} ion conductivity in the fully dehydrated C12A7 at 1350 °C. The conductivity difference between the proton and the O^{2-} ion diffusions increases with decreasing temperature or decreasing degree of hydration. Thus, in the oxidizing atmosphere, the total electrical conductivity of C12A7 is always dominated by O^{2-} ion conduction, and degradation of the oxide ion conductivity in a wet atmosphere[10] is ascribed to the decrease of the extra-framework O^{2-} ion concentration due to the alternative formation of OH^- ions.

5. Conclusion

By combined analysis of IR spectroscopy for OH^- band with thermodynamics for the OH^- formation process, we obtained $1.31 \pm 0.04 \times 10^3\ M^{-1}{\cdot}cm^{-2}$ for the molar integral extinction coefficient of the OH-stretching band and $-228 \pm 20\ kJ{\cdot}mol^{-1}$ for the enthalpy of the hydration. This extremely high hydration enthalpy in C12A7 is associated with the instability of the extra-framework O^{2-} ions, leading to an unusually high dehydration temperature, e.g., ~1200 °C under $p(H_2O) = 0.02$ atm. It was confirmed that hydration in C12A7 is mediated by the reaction between an extra-framework O^{2-} ion with a H_2O molecule at the surface and by the incorporation of the extra-framework OH^- ions in bulk accompanied by the ambipolar diffusion of the O^{2-} and OH^- ions. The rate-determination process is the inward bulk diffusion of OH^- ions, whose diffusivity is at least 2 orders of magnitude less than the O^{2-} diffusivity. As a consequence, oxide ion conductivity of C12A7 is decreased by hydration.

Acknowledgment. This work was supported by the Grant-in-Aid for Creative Scientific Research (No. 16GS0205) from the Japanese Ministry of Education, Culture, Sports, Science and Technology.

Appendix

Fluxes of diffusing species are expressed as

$$j_{H_2O} = -\frac{c_{H_2O}\tilde{D}_{H_2O}}{RT}\nabla\mu_{H_2O} \quad \text{(A1)}$$

$$j_{OH^-} = -\frac{c_{OH^-}D_{OH^-}}{RT}(\nabla\mu_{OH^-} + F\nabla\phi) \quad \text{(A2)}$$

$$j_{O^{2-}} = -\frac{c_{O^{2-}}D_{O^{2-}}}{RT}(\nabla\mu_{O^{2-}} + 2F\nabla\phi) \quad \text{(A3)}$$

where c is the concentration, D is the diffusion coefficient, μ is the chemical potential, F is the Faraday constant, ϕ is the electrostatic potential, and subscripts specify diffusing species. Charge neutrality and chemical equilibrium conditions derived from eq 3 gives

$$j_{H_2O} = 1/2 j_{OH^-} = -j_{O^{2-}} \quad \text{(A4)}$$

$$\nabla\mu_{H_2O} = 2\nabla\mu_{OH^-} - \nabla\mu_{O^{2-}} \quad \text{(A5)}$$

By eliminating F, ϕ, j_{OH^-}, and $j_{O^{2-}}$ using eqs A1−5, one obtains

$$j_{H_2O} = -\frac{2c_{OH^-}D_{OH^-}c_{O^{2-}}D_{O^{2-}}}{8c_{O^{2-}}D_{O^{2-}} + c_{OH^-}D_{OH^-}} \cdot \frac{\nabla\mu_{H_2O}}{RT} \quad \text{(A6)}$$

Charge neutrality condition gives

$$2c_{H_2O} = c_{OH^-} = 2(c_a - c_{O^{2-}}) \quad \text{(A7)}$$

Then, eq A6 is rewritten as

$$j_{H_2O} = -\frac{(c_a - c_{H_2O})D_{OH^-}D_{O^{2-}}}{2(c_a - c_{H_2O})D_{O^{2-}} + c_{H_2O}D_{OH^-}} \cdot \frac{c_{H_2O}\nabla\mu_{H_2O}}{RT} \quad \text{(A8)}$$

From Eqs. A1 and A8, one obtains,

$$\tilde{D}_{H_2O} = \frac{(c_a - c_{H_2O})D_{OH^-}D_{O^{2-}}}{2(c_a - c_{H_2O})D_{O^{2-}} + c_{H_2O}D_{OH^-}} \quad \text{(A9)}$$

Provided that $c_{H_2O} < c_a$ and $D_{OH^-} \ll D_{O^{2-}}$, D_{OH^-} is approximated as

$$D_{OH^-} \approx 2\tilde{D}_{H_2O} \quad \text{(A10)}$$

References and Notes

(1) Jeevaratnam, J.; Glasser, L. S. D.; Glasser, F. P. *Nature* **1962**, *194*, 764−765. Nurse, R. W.; Welch, J. H.; Majumdar, A. J. *Trans. Br. Ceram. Soc.* **1965**, *64*, 323−332. Imlach, J. A.; Glasser, L. S. D.; Glasser, F. P. *Cement Conc. Res.* **1971**, *1*, 57−61.; Singh, V. K.; Glasser, F. P. *Ceram. Int.* **1988**, *14*, 59−62.

(2) Bartl, H.; Scheller, T. *N. Jb. Miner. Mh.* **1970**, *35*, 547−552.

(3) Jeevaratnam, J.; Glasser, F. P, Glasser, L. S. D. *J. Am. Ceram. Soc.* **1964**, *47*, 105−106.

(4) Hosono, H.; Abe, Y. *Inorg. Chem.* **1987**, *26*, 1192−1195. Stösser, R.; Nofz, M.; Gessner, W.; Schröter, C.; Kranz, G. J. *Solid State Chem.* **1989**, *81*, 152−164. Matusishi, S.; Hayashi, K.; Hirano, M.; Hosono, H. *J. Phys. Chem. B* **2004**, *108*, 18557−18568.

(5) Hayashi, K.; Hirano, M.; Matsuishi, S.; Hosono, H. *J. Am. Chem. Soc.* **2002**, *124* 738−739. Hayashi, K.; Matsuishi, S.; Ueda, N.; Hirano, M.; Hosono, H. *Chem. Mater.* **2003**, *15*, 1851−1854.

(6) Hayashi, K.; Matsuishi, S.; Kamiya, T.; Hirano, M.; Hosono, H. *Nature* **2002**, *419*, 462−465.

(7) Zhmoidin, G. I.; Chatterjee, A. K. *Cement Conc. Res.* **1984**, *14*, 386−396.

(8) Formation in glassy phase, Kim, S.-W.; Miyakawa, M.; Hayashi, K.; Sakai, T.; Hirano, M.; Hosono, H. *J. Am. Chem. Soc.* **2005**, *127*, 1370−1371.

(9) Matsuishi, S.; Toda, Y.; Miyakawa, M.; Hayashi, K.; Kamiya, T.; Hirano, M.; Tanaka, I.; Hosono, H. *Science* **2003**, *301*, 626−629. Sushiko, P. V.; Shluger, A. L.; Hayashi, K.; Hirano, M.; Hosono, H. *Phys. Rev. Lett.* **2003**, *91*, 126401−4.

(10) Lacerda, M.; Irvine, J. T. S.; Glasser, F. P.; West A. R. *Nature* **1988**, *332*, 525−526. Irvine J. T. S.; Lacerda, M.; West, A. R. *Mater. Res. Bull.* **1988**, *23*, 1033−1038.

(11) Li, Q.; Hayashi, K.; Nishioka, M.; Kashiwagi, H.; Hirano, M.; Torimoto, Y.; Hosono, H.; Sadakata, M. *Appl. Phys. Lett.* **2002**, *80*, 4259−4261. Hayashi, K.; Li, Q.; Nishioka, M.; Matsuishi, S.; Torimoto, Y.; Hirano, M.; Sadakata, M.; Hosono, H. *Electrochem. Solid-State Lett.* **2002**, *5*, J13−J16. Li, Q.; Hayashi, K.; Nishioka, M.; Kashiwagi, H.; Hirano, M.; Torimoto, Y.; Hosono, H.; Sadakata, M. *Jpn. J. Appl. Phys.* **2002**, *41*, L530−L532. Li, Q.; Hosono, H.; Hirano, M.; Hayashi, K.; Nishioka, M.; Kashiwagi, H.; Torimoto, Y.; Sadakata, M. *Surf. Sci.* **2003**, *527*, 100−112.

(12) Toda, Y.; Matsuishi, S.; Hayashi, K.; Ueda, K.; Kamiya, T.; Hirano, M.; Hosono, H. *Adv. Mater.* **2004**, *16*, 685−689.

(13) Hayashi, K.; Toda, Y.; Kamiya, T.; Hirano, M.; Yamanaka, M.; Tanaka, I.; Yamamoto, T.; Hosono, H. *Appl. Phys. Lett.* **2005**, *86*, 022109−3.

(14) Hayashi, K.; Hirano, M.; Hosono, H. *J. Mater. Res.* **2002**, *17*, 1244−1247.

(15) Miyakawa, M.; Toda, Y.; Hayashi, K.; Hirano, M.; Kamiya, T.; Matsunami, N.; Hosono, H. *J. Appl. Phys.* **2005**, *97*, 023510−6.

(16) McMillan, P.; Piriou, B. *J. Non-Cryst Solids* **1983**, *55*, 221−242.

(17) Crank, J. The Mathematics of Diffusion, 2nd ed.; p 91, Oxford Science Publications: Oxford, 1975.

(18) Hayashi, K.; Matsuishi, S.; Hirano, M.; Hosono, H. *J. Phys. Chem. B.* **2004**, *108*, 8920−25. Hayashi, K.; Ueda, N.; Hirano, M.; Hosono, H. *Solid State Ionics* **2004**, *173*, 89−94.

(19) Mitachi, S.; Fonteneau, G.; Christensen, P. S.; Lucas, J. *J. Non-Cryst. Solids* **1987**, *92*, 313−325.

(20) Wedding, B.; Klein, M. V. *Phys. Rev.* **1969**, *177*, 1274−1288.

(21) Johnson, O. W.; DeFord, J., Shaner, J. W. *J. Appl. Phys.* **1973**, *44*, 3008−3012.

(22) Shelby, J. E.; Vitko, J.; Benner, R. E. *J. Am. Ceram. Soc.* **1982**, *65*, C59−C60.

(23) Hayashi et al., unpublished work.

(24) Kreuer, K. D. *Solid State Ionics* **1997**, *97*, 1−15. Kreuer, K. D. *Solid State Ionics* **1999**, *125*, 285−302.

(25) Calculated using Malt program, Kagaku Gijutsu-Sha, Japan; Yokokawa H.; Yamauchi, S.; Matsumoto, T. *Calphad* **2002**, *26*, 155−166.

(26) Rritz, B.; Luty, F.; Anger, J. *Z. Physik* **1963**, *174*, 240−256.

(27) Muller, R.; Gunthard, H. *J. Chem. Phys.* **1966**, *44*, 365−373.

(28) Mitachi, S.; Sakaguchi, S.; Takahashi, S. *Phys. Chem. Glass.* **1986**, *27*, 144−146.

(29) Morimoto, Y.; Nozawa, S.; Hosono, H. *Phys. Rev. B* **1999**, *59*, 4066−4073.

(30) Fioretto, D.; Freda, M.; Onori, G.; Santucci, A. *J. Phys. Chem. B* **1999**, *103*, 8216−8220.